First Principles and Finite Element Predictions of Radiative Properties of Nanostructure Arrays: Single-Walled Carbon Nanotube Arrays

Aaron Sisto[1]
School of Mechanical Engineering and
Birck Nanotechnology Center,
Purdue University,
West Lafayette, IN 47907

Xiulin Ruan[2]
School of Mechanical Engineering and Birck
Nanotechnology Center,
Purdue University,
West Lafayette, IN 47907
e-mail: ruan@purdue.edu

Timothy S. Fisher
School of Mechanical Engineering and
Birck Nanotechnology Center,
Purdue University,
West Lafayette, IN 47907

Recent advances in nanofabrication technology have facilitated the development of arrays of nanostructures in the classical or quantum confinement regime, e.g., single-walled carbon nanotube (SWCNT) arrays with long-range order across macroscopic dimensions. So far, an accurate generalized method of modeling radiative properties of these systems has yet to be realized. In this work, a multiscale computational approach combining first-principles methods based on density functional theory (DFT) and classical electrodynamics simulations based on the finite element method (FEM) is described and applied to the calculations of optical properties of macroscopic SWCNT arrays. The first-principles approach includes the use of the GW approximation and Bethe–Salpeter methods to account for excited electron states, and the accuracy of these approximations is assessed through evaluation of the absorption spectra of individual SWCNTs. The fundamental mechanisms for the unique characteristics of extremely low reflectance and high absorptance in the near-IR are delineated. Furthermore, opportunities to tune the optical properties of the macroscopic array are explored. [DOI: 10.1115/1.4026552]

Keywords: thermal radiative properties, first principles, finite element, carbon nanotubes

Introduction

Recent advances in nanofabrication technology have facilitated the development of nanostructure arrays in which each individual nanostructure has a size in the classical or quantum confinement regime, such as silicon nanowire arrays [1], carbon nanotube arrays [2], and quantum dot arrays [3], to name a few. These hierarchical nanostructures have potential applications in photovoltaics, photocatalysis, solar-thermal, and radiative thermal management, among others. Understanding radiative properties of such nanostructure arrays requires an understanding of the behavior of each individual nanostructure as well as the effects of the long-range order or disorder [4,5].

Among these nanostructure arrays, vertically oriented SWCNT arrays have been synthesized with long-range order across macroscopic dimensions [6,7]. These arrays exhibit a wide range of optical properties as a result of the unique structure and electronic properties of individual CNTs, as well as the periodicity and chirality distributions inherent in macroscopic arrays [8–10]. CNT arrays have been found to exhibit extremely low reflectance ($<2\%$) over a wide spectral range [2,11]. These arrays are characterized as having low volumetric density, with a volume fraction of approximately 3%, corresponding to an intertube separation of $\sim$15 nm. The average diameter of the SWCNTs in the arrays varies depending on fabrication technique and application, but has been reported to fall in the range of 0.4–2.0 nm [12–14]. Furthermore, the exceptionally high spectral and directional absorption in the near-IR and visible spectra enables CNT arrays to exhibit nearly blackbody characteristics. The fundamental mechanisms leading to these unique properties are still not well understood. The potential for optimization of array parameters such as thickness and density motivates a rigorous fundamental study of the electrodynamics of this class of nanostructured metamaterials.

Classical electrodynamics simulations have been used to calculate optical properties of multi-walled carbon nanotube (MWCNT) arrays, as well as to examine field propagation effects related to the structure of the material [4,15]. However, the major issue in the use of electrodynamics simulations to examine structures at the nanoscale is the application of the bulk dielectric function to dimensions at which this intrinsic material property is no longer valid. As a result of the 1D structure and electronic properties of SWCNTs, the dielectric function is known to deviate significantly from that of graphite or MWCNTs [16], and exhibits strong dependence on diameter and chirality [17]. Without experimental measurements of the dielectric function for specific SWCNT chiralities, these materials cannot be accurately modeled by classical electrodynamics alone.

In the present work, we report on the development of a multiscale approach for thermal radiation, accounting for the specific atomic structure of individual CNTs and many-body effects. The incorporation of the electronic structure of each individual nanostructure is necessary to yield an effective dielectric response function that accurately describes the overall response of the arrays considered here. We use a first-principles quantum-mechanical approach based on DFT to calculate the dielectric tensor for individual SWCNTs, explicitly treating the electron-hole interaction and accounting for excitonic effects that have been shown to be significant in materials of reduced dimensions, and specifically CNTs [18]. In this approach, we characterize the electronic ground state using DFT; quasi-particle energies are calculated within the GW approximation; and the coupled electron-hole excitation energies and optical spectrum are obtained by solving the Bethe–Salpeter equation (BSE). The GW-BSE framework has

[1]Current address: School of Materials Science and Engineering, Stanford University, Stanford, CA 94305.
[2]Corresponding author.

Contributed by the Heat Transfer Division of ASME for publication in the Journal of Heat Transfer. Manuscript received June 24, 2012; final manuscript received January 18, 2014; published online March 10, 2014. Assoc. Editor: He-Ping Tan.

been shown to reproduce experimental results accurately for a wide range of materials, including SWCNTs [19,20]. The dielectric tensors of individual CNTs calculated from the solution of the BSE are input into electrodynamics simulations as intrinsic material properties describing the CNTs. The solution of Maxwell's equations for a periodic, inhomogeneous, vertically aligned SWCNT array then provides the effective optical properties of the macroscopic array.

The novelty of this method lies in the encapsulation of highly accurate electronic structure methods within electrodynamics simulations to understand and predict optical phenomena in nanostructured materials. These observed properties, such as absorptance and reflectance, which describe a material's interaction with different wavelengths of light, can begin to appear at macroscopic structural dimensions of nanometers, but arise uniquely from the quantum-mechanical effects associated with the underlying atomic structure of the material. Classical electrodynamics simulations of such nanostructured materials can only be accurate if the description of the material properties reflects these quantum-mechanical characteristics of the dielectric response function. Electronic structure methods are confined to relatively small systems, on the scale of hundreds to thousands of atoms, while classical electrodynamics simulations are typically conducted at the continuum scale. Many electrodynamics methods have been developed to efficiently solve for radiative properties of both randomly distributed and periodic structures (e.g., Ref. [21]). Similarly, electronic structure methods have evolved to characterize the ground and excited states of a wide range of systems [22,23]. However, excited-state methods often incur much higher computational cost if accuracy is required. Methods such as time-dependent density functional theory [24] have become popular due to favorable degrees of accuracy and computational expense, but large errors in excitation energies are still prevalent, relative to experiments. In the proposed methodology, the dielectric function calculated at the electronic structure level must be extremely accurate as it directly influences the behavior of the macroscopic material as it interacts with light. In general, the calculation of the dielectric function using first-principles is very computationally expensive relative to the electrodynamics simulations.

Although SWCNT arrays provide a prototypical system for validation of this method, the underlying components of the multiscale method remain general in the sense that an arbitrary atomic scale structure can be treated within the GW-BSE framework and its dielectric function can then be used to describe general microscopic structures within classical electrodynamics. Thus, both atomic structure and macroscopic design spaces can be explored by this predictive method, facilitating more efficient design and materials discovery compared to purely experimental methods.

Methodology

The SWCNT array structure under consideration is sketched in Fig. 1. Since precise control of chirality in macroscopic SWCNT arrays is still elusive in experiments, the inhomogeneity inherent in macroscopic arrays must be accounted for in order to understand and optimize the optical properties of the array. We consider a normal distribution of SWCNTs with mean diameter 0.7 nm and standard deviation 0.2 nm. These diameters fall within the range of diameters reported in fabrication and measurements of optical properties. The chiralities are chosen in consideration of computational cost to be either armchair or zigzag due to their decreased unit cell size, and they are (11-0), (10-0), (8-0), and (6-6). For a vertical array with equal CNT length, the incident angle θ is defined as the angle between the incidence and the surface normal of the array (or the axial direction of CNTs). The s-polarization is defined as when the electric field of the light is parallel to the CNT axis, while the p-polarization is when the electric field is perpendicular to the CNT axis. The individual dielectric tensors of a set of SWCNTs with varying chirality are calculated from first-principles. The dielectric tensors of the CNTs are then used

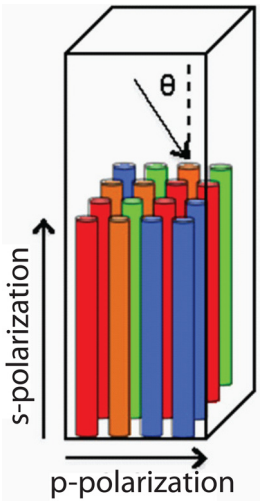

Fig. 1 A sketch of the SWCNT array structure and the incident angles θ

in electrodynamics simulations of the macroscopic array. In this way, the optical properties of the macroscopic array can be calculated for a specified array geometry.

The first-principles approach initially involves the calculation of the ground-state wavefunctions and eigenvalues of the Kohn-Sham equations within the local density approximation (LDA). We use a planewave basis with a cutoff of 100 Ry and Troullier-Martins norm-conserving pseudopotentials [25], with a convergence threshold of 1×10^{-6} Ry for self-consistency. At least 10 Å vacuum space is included in the radial directions to minimize interactions with periodic images. 32 k-points are used for the DFT and GW calculations, and 400 k-points are used in the BSE calculations. The long-range coulomb interaction arising from the 1D structure of CNTs is truncated based on a cylindrical geometry that has been documented previously [26]. This is done to ensure that intertube interactions do not influence the calculated dielectric function because the intertube separation in experiments is much larger than the characteristic CNT diameter. The solution of Maxwell's equations subject to boundary conditions forms the basis of electrodynamics simulations. Here, we use the FEM to solve these equations in the differential form for a time-varying electric field in three-dimensional space.

The coupling between the first-principles calculations and electrodynamics simulations can be defined explicitly by relating the electric displacement to the electric field

$$D_i(\boldsymbol{r},\omega) = \sum_j \varepsilon_{ij}(\boldsymbol{r},\omega) E_i(\boldsymbol{r},\omega) \tag{1}$$

where $\varepsilon(\omega)$ is the complex, frequency-dependent dielectric tensor. The imaginary part of the dielectric tensor component ε_{ij} is calculated within the GW-BSE method as

$$\varepsilon''_{ij}(\omega) = \frac{16\pi e^2}{\omega^2} \sum_S \left| \lambda_{ij} \cdot 0 | \vec{v} | S \right|^2 \delta(\omega - \Omega_S) \tag{2}$$

where λ is the polarization vector, ν is the single-particle velocity operator, and Ω_S is the excitation energy. The real part of the relative permittivity is then calculated using the well-known Kramers-Kronig relations. The low dimensionality of the CNT structure and associated variation in the relative localization of electronic states parallel and perpendicular to the tube axis necessitates the calculation of the diagonal frequency-dependent elements of the dielectric tensor from first-principles.

The real and imaginary parts of the index of refraction and are calculated from the usual expressions from classical electrodynamics

$$n = \sqrt{\frac{\sqrt{\varepsilon_1^2 + \varepsilon_2^2} + \varepsilon_1}{2}} \tag{3}$$

$$k = \sqrt{\frac{\sqrt{\varepsilon_1^2 + \varepsilon_2^2} - \varepsilon_1}{2}} \tag{4}$$

where ε_1 and ε_2 are the real and imaginary parts of the dielectric function. Electrodynamics simulations are performed with light incident on an array. The macroscopic array is treated as a homogeneous, effective material, with the effective dielectric tensor defined within Maxwell–Garnett (MG) effective medium theory [27]. The MG expression for the effective relative permittivity is

$$\varepsilon_{\text{eff},k} = \varepsilon_0 + \frac{\sum_i \frac{f_i(\varepsilon_i - \varepsilon_0)}{\varepsilon_0 + N_{i,k}(\varepsilon_i - \varepsilon_0)}}{1 - \sum_i N_{i,k} \frac{f_i(\varepsilon_i - \varepsilon_0)}{\varepsilon_0 + N_{i,k}(\varepsilon_i - \varepsilon_0)}} \tag{5}$$

where the background permittivity, ε_0, is taken to be that of vacuum. The summation is over all CNTs included in the effective material, with f being the volume fraction of each index, k, corresponding to the light polarization vector. N is the depolarization factor, which depends on the polarization of light and the geometry of the dielectric inclusion. Here, it is taken to be $1/2$ for s-polarization and zero for p-polarization, as analytically for a thin rod geometry. The use of MG theory was validated by comparing the calculated absorption spectra of the effective material with that of an inhomogeneous array with the geometry of individual CNTs defined using a Monte Carlo method of randomization. Both treatments of the macroscopic array account for inhomogeneity in the spatial CNT distribution and assume well-ordered arrays with the CNT axes perfectly aligned. Due to the absence of classical resonance effects, it was found that the calculated absorption spectra were identical. The effective medium approach was used in all subsequent results, as it is significantly less computationally expensive than the Monte Carlo approach.

Results

The dielectric tensors are calculated for all chiralities within the GW-BSE method, and the resulting imaginary and real parts for the s-polarization are shown in Fig. 2. The imaginary part of the dielectric function for s-polarization of the semiconducting (8,0) CNT has been calculated previously with the GW-BSE method [16], and the present results are found to be almost identical. It has been shown previously that DFT significantly underpredicts the band gap of most semiconducting bulk materials as well as reduced dimensionality structures such as semiconducting CNTs. This is a result of the approximation to the exchange-correlation potential, which is necessary to use because the exact exchange-correlation potential is not known. However, GW acts to widen the bandgap by accounting for quasi-particle effects and essentially "corrects" the DFT one-electron energies. Subsequently, BSE accounts for the electron-hole interaction and thus reduces the band gap by an amount equivalent to the exciton binding energy. The first and second peaks in Fig. 2(*b*) calculated from GW-BSE agree very well with experiments [28], validating the use of this first-principles method (Table 1). For the metallic (6,6) SWCNT, we observe a 15% increase in the slope of the dispersion relation of the quasi-particle bands relative to the LDA results. The exciton binding energy is approximately 60 meV. This is in agreement with GW-BSE calculations of other small-diameter, metallic SWCNTs [29]. Figure 2 reveals strong absorption peaks in the near IR and visible spectra for s-polarization. Further, the absorption peaks for the (6,6) metallic CNT are higher in energy than those of the semiconducting CNTs. Previous tight binding calculations have shown that the first absorption peaks of metallic CNTs are higher in energy than those of semiconducting CNTs of similar diameter [30].

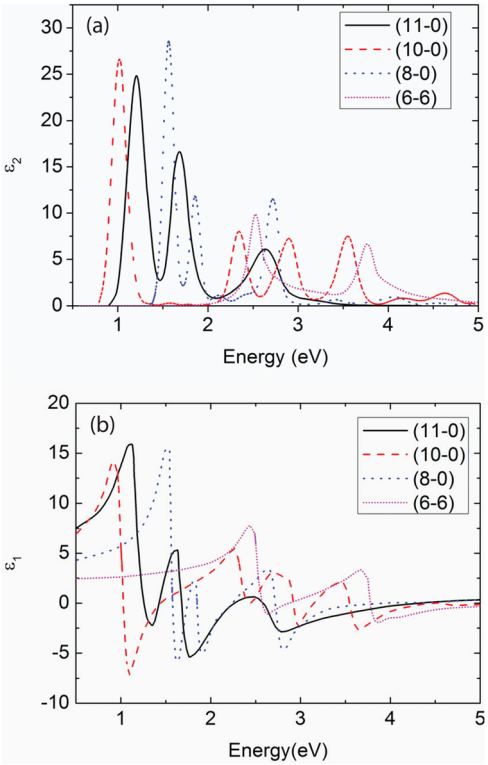

Fig. 2 GW-BSE dielectric function of SWCNTs for the s-polarization: (*a*) imaginary part and (*b*) real part, with a broadening of 0.80 eV

Table 1 Energetic positions of first and second absorption peaks for the s-polarization

	GW-BSE (E_{11}, E_{22}) (eV)	Exp. (E_{11}, E_{22}) (eV) [28]
(11,0)	1.18, 2.67	1.21, 2.69
(10,0)	1.01, 2.34	1.11, 2.36
(8,0)	1.56, 1.85	1.62, 1.88
(6,6)	2.53, 3.77	

The optical response for the p-polarization is shown in Fig. 3, where it can be seen that the depolarization effects cause the CNT optical response to be significantly suppressed [31,32]. As a result, the optical transitions at lower energies are forbidden, resulting in

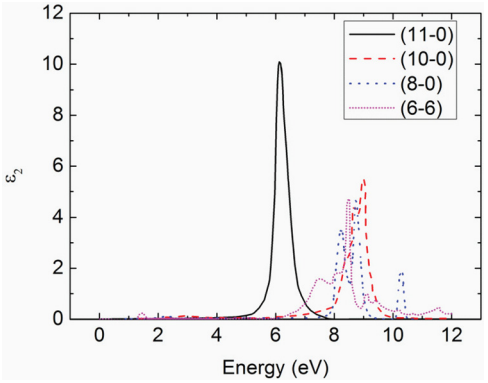

Fig. 3 GW-BSE imaginary part of the dielectric function of SWCNTs for the p-polarization with a broadening of 0.80 eV

absorption peaks in the UV spectrum (Fig. 3). Conceptually, the drastic difference in absorption band edge between s- and p-polarizations arises from the relative localization of electronic states in the axial and radial directions and the associated restrictions on the ground-state polarizability tensor. These characteristics of the anisotropy in the dielectric functions of SWCNTs have been observed previously in theory and experiment [33,34].

The use of the MG theory has been shown to be valid because the large intertube separation relative to the characteristic SWCNT diameter prevents resonance effects from contributing to the optical properties [35,36]. The inhomogeneity in the CNT distribution is accommodated in MG theory simply through the volume fraction corresponding to each CNT in the array. The volume fraction of the (6,6) metallic CNT was varied between 10% and 50% due to the fact that in practice this quantity is sensitive to the synthesis technique; general CNT growth processes produce arrays with approximately 33% metallic CNTs [36]. The volume fractions of the three semiconducting CNTs were set equal to each other such that the total volume fraction of CNTs defined the desired array density. This quantity was set to 3% to simulate relevant experimental conditions for SWCNT arrays [11]. As the number of metallic CNTs increases, with the total CNT density fixed, the intensity of absorption peaks in the visible spectrum increase relative to those in the near IR (Fig. 4(*a*)). This is due to the fact that the absorption peaks for the (6,6) metallic CNTs exist at higher energy than those of semiconducting CNTs, as discussed above. This result presents the opportunity to tune the optical properties of the array to selectively increase absorption in a specific spectrum by altering the number of metallic CNTs during the synthesis process. The density of metallic CNTs relative to the total number of CNTs was fixed at 33% for all subsequent calculations.

The optical properties of the macroscopic array have been calculated for an incidence angle of 45 deg and array thickness 1 μm, and the calculated radiative properties (absorptance, reflectance, and transmittance) are shown in Fig. 4(*b*). The absorption and transmission clearly dominate the response of the material, with reflectance remaining below 2% over the entire spectral range. The peaks and shoulders in the absorptance relate directly to peaks in the calculated ε_2 for both polarizations resulting from components of the electric field both parallel and perpendicular to the CNT axis. The absorption at energies below 5 eV corresponds to peaks in ε_2 for s-polarization, whereas the peak at 7 eV is attributed to the peak in ε_2 for p-polarization.

The reflectance of a vertically aligned array is dominated by the response to p-polarized light. The reflectance of p-polarized light can be explained by the effective refractive index from the real and imaginary parts of the effective dielectric function for the p-polarization. Figure 4(*c*) shows the effective refractive index with varying CNT density, with the 3% volume fraction corresponding to an intertube separation of 15 nm, and the higher density corresponding to an intertube separation of 4 nm. The extremely low index of refraction is unusual for natural materials and results from the array's sparsely aligned nanostructures. For p-polarized light, the effective refractive index close to that of air at lower frequencies leads to low reflectance. Its low absorption due to weak optical response indicates that the material is significantly more transparent to this polarization than to s-polarization. Therefore, the p-polarized component of light is able to propagate through the material while the s-polarized component is absorbed. It is apparent that as the density increases, the index of refraction for p-polarized light increases, leading to an overall increase in the reflectance.

The effects of light polarization on the blackbody behavior of the material are examined by varying the incidence angle between 0 and 90 deg, and the results are shown in Fig. 5. Although these results are for a particular frequency of 1 eV, the reflectance does not significantly differ over the entire spectrum. For normal incidence, the light only has the p-polarization, and the reflectance is given by the Fresnel's equation

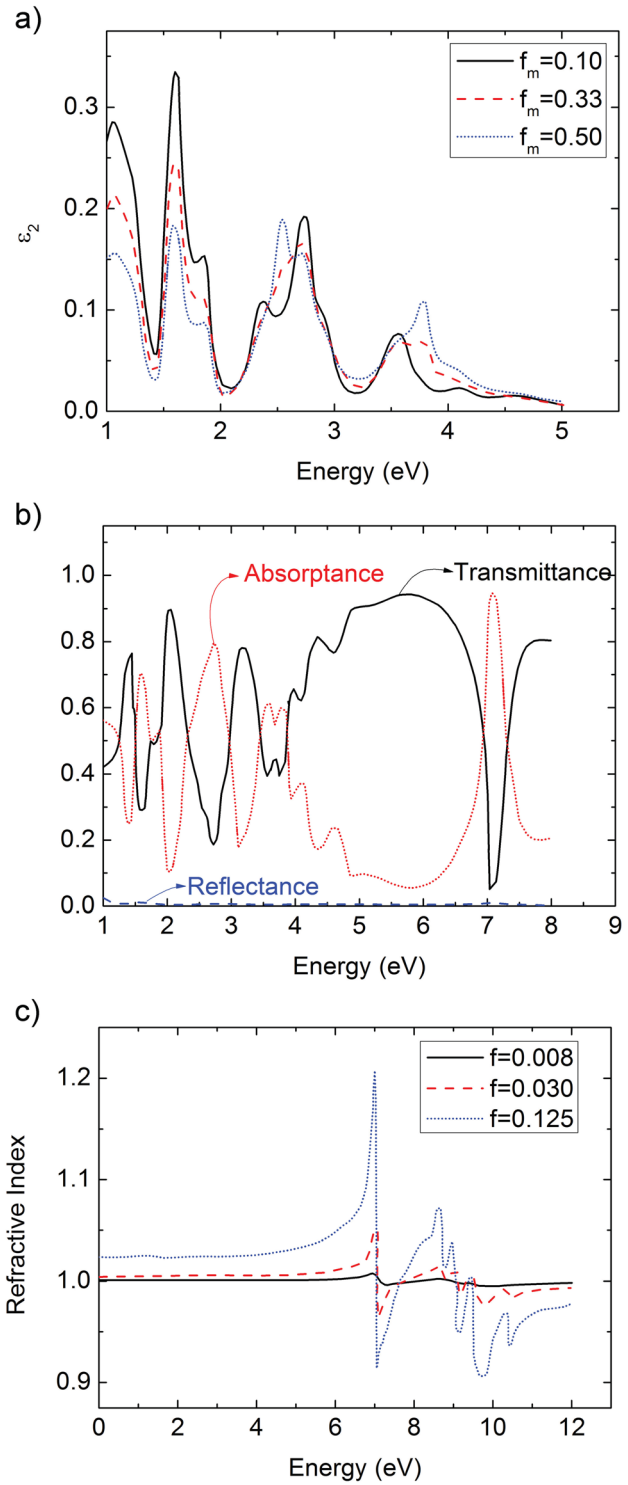

Fig. 4 (*a*) Imaginary part of the dielectric function for s-polarized light with varying fraction of metallic CNTs, f_m, relative to the total number of CNTs, (*b*) effective optical properties of 1 μm thick slab and incidence angle of 45 deg, and (*c*) effective real index of refraction for a macroscopic array for the p-polarized light

$$R = \left|\frac{n_1 - n_2}{n_1 + n_2}\right|^2 \tag{6}$$

At normal incidence, the effective index of refraction is converged to 1.005 as the frequency decreases below the first absorption peak at 7 eV, which is extremely close to that of air. This

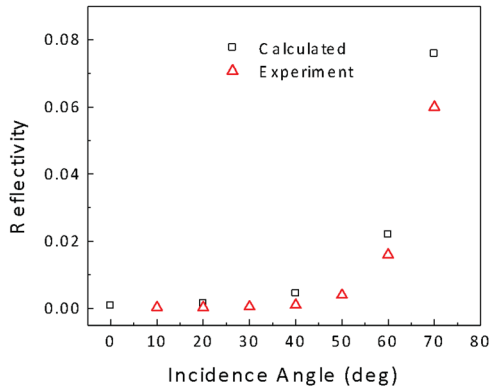

Fig. 5 Predicted reflectance of the macroscopic array as a function of incidence angle, as well as the measured spectral reflectance data from Ref. [11]. Both calculations and experiments refer to a vertically aligned array with tilt angle of 20 deg.

leads to a reflectance to 2.5×10^{-6}. As the incident angle increases, the reflectance also increases. The calculated reflectance curve agrees well with experiment [12]. The simulations account for a 20 deg tilt in the CNT alignment relative to the surface normal as is described in the experiment. It is reasonable that the reflection increases with the incidence angle because the s-polarization component increases and electrons are able to couple to the light to a much higher degree. Minor discrepancies between theory and experiment in Fig. 5 could be attributed to imperfections in the experimental CNT array. Disorder in the alignment, assumed perfect in simulations, as well as variations in CNT chirality not included in the model are expected to alter the optical properties to a low degree. The agreement here suggests that the optical properties are not as strongly dependent on CNT chirality as the array structure and general features of the effective dielectric tensor.

As a necessary condition for the CNT arrays to be strong optical absorbers, the absorption must be significantly higher than the transmission to eliminate the dependence of the optical properties on interactions with the substrate. Therefore, the variation of the optical properties with respect to array thickness is investigated here by varying the length of the material in the surface normal direction. The calculated absorptance is shown with varying array thickness in Fig. 6(*a*). As the thickness increases, the absorptance increases significantly, resulting in a decrease in the transmittance over the entire spectrum, with the reflectance remaining nearly constant. The change in absorbance (related to transmittance T as $\log_{10}(1/T)$) as a function of array thickness is also shown in Fig. 6(*b*) for light at frequency of 2.5 eV, corresponding to experiment [37]. A linear trend is observed as the thickness increases, in qualitative agreement with the experiment. Although both theory and experimental plots indicate that absorbance varies approximately linearly with thickness, a linear fit to the data results in a slope of 0.5 ($1/\mu$m) in experiments and 0.14 ($1/\mu$m) in simulations. The difference is due to the large differences between mean nanotube diameter in the experiment and simulation. The experimental array contains SWCNTs with diameters ranging from 0.5 to 1.5 nm, resulting in large variations in the effective dielectric function, especially at the selected light frequency. For the much narrower diameter distribution of the simulation relative to experiment, the transmittance decreases much more quickly as the absorption is enhanced at energetically localized absorption peaks.

These results suggest that the low spectral reflectance and high absorptance of these materials is a direct result of both the atomic and microscopic structure of the CNTs and array, respectively. The individual CNTs absorb s-polarized light strongly in the near IR and visible spectra and have a much weaker optical response to p-polarized light. However, it is the sparse array geometry that

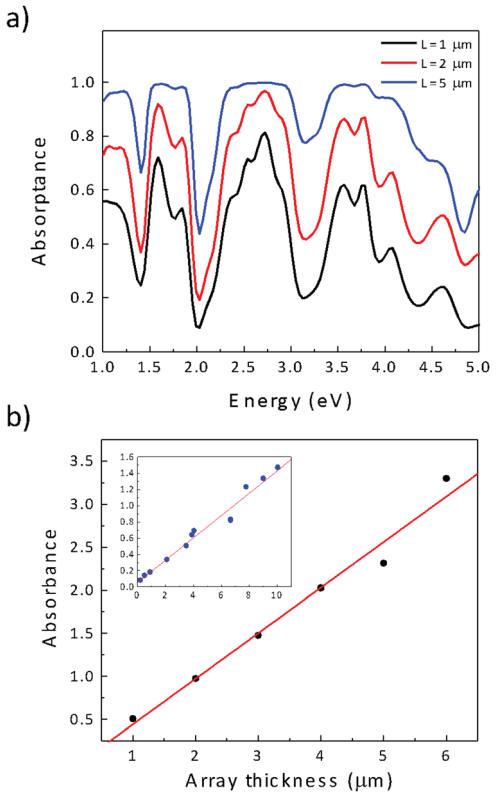

Fig. 6 (*a*) Calculated absorptance for varying array thickness and (*b*) absorbance of the macroscopic array as a function of array thickness. The inset is the measured absorbance corresponding to experiments in Ref. [37]. Both experiment and theory correspond to a wavelength of 488 nm.

causes the reflectance to remain significantly lower than other materials. As discussed previously, the effective material is virtually transparent to p-polarized light, but strongly absorbs s-polarized light. Because of the low CNT density, the index of refraction for p-polarized light is significantly lower than that of other low index of refraction materials. This property decreases reflection of light in the surface normal direction and allows the light to propagate through the material and gradually become absorbed. This phenomenon confirms the importance of CNT length on the high absorption observed in experiment. Furthermore, the alignment of the CNTs establishes a clear relationship between the anisotropy of the individual CNTs and that of the macroscopic array. Disorder in the vertical orientation of individual CNTs in the array would result in increased reflection due to mixing of the absorptive and transparent elements in the dielectric tensor.

Conclusions

We have developed a multiscale computational method, by combining ab initio calculations and finite element electrodynamics methods, to predict the optical properties of inhomogeneous nanostructure arrays. This method, applied to the properties of macroscopic SWCNT arrays, has resulted in a fundamental understanding of the mechanisms leading to the unique blackbody behavior of the material. The computed properties of the array are in agreement with previous experiments, and the simulations have been used to suggest means to modify the effective optical properties based on systematic variation of geometric parameters of the array.

Acknowledgment

This project was partially supported by the Air Force Office of Scientific Research through the Discovery Challenge Thrust

program. A.S. also acknowledges the DOE Computational Science Graduate Fellowship and the Molecular Foundry Program. We gratefully appreciate Dr. Jeffrey Neaton for his help. We also thank Yan Wang for assistance in plotting the figures.

Nomenclature

$\boldsymbol{D}$ = displacement field
$\boldsymbol{E}$ = electric field
F = fill factor
k = imaginary part of index of refraction
N = depolarization factor
n = real part of index of refraction
R = reflectivity
$\boldsymbol{r}$ = position
v = velocity
$\boldsymbol{\varepsilon}$ = dielectric function
ε_0 = vacuum permittivity
ε', ε_1 = real part of dielectric function
ε'', ε_2 = imaginary part of dielectric function
λ = polarization vector
Ω = excitation energy
ω = frequency

Subscripts

i, j = row, column index of tensor

References

[1] Tsakalakos, L., Balch, J., Fronheiser, J., Korevaar, B. A., Sulima, O., and Rand, J., 2007, "Silicon Nanowire Solar Cells," Appl. Phys. Lett., **91**(23), p. 233117.
[2] Yang, Z. P., Ci, L. J., Bur, J. A., Lin, S. Y., and Ajayan, P. M., 2008, "Experimental Observation of an Extremely Dark Material Made by a Low-Density Nanotube Array," Nano Lett., **8**(2), pp. 446–451.
[3] Nozik, A. J., Beard, M. C., Luther, J. M., Law, M., Ellingson, R. J., and Johnson, J. C., 2010, "Semiconductor Quantum Dots and Quantum Dot Arrays and Applications of Multiple Exciton Generation to Third-Generation Photovoltaic Solar Cells," Chem. Rev., **110**(11), pp. 6873–6890.
[4] Bao, H., Ruan, X. L., and Fisher, T. S., 2010, "Optical Properties of Ordered Vertical Arrays of Multi-Walled Carbon Nanotubes From FDTD Simulations," Opt. Express, **18**(6), pp. 6347–6359.
[5] Bao, H., and Ruan, X. L., 2010, "Optical Absorption Enhancement in Disordered Vertical Silicon Nanowire Arrays for Photovoltaic Applications," Opt. Lett., **35**(20), pp. 3378–3380.
[6] Maschmann, M. R., Franklin, A. D., Amama, P. B., Zakharov, D. N., Stach, E. A., Sands, T. D., and Fisher, T. S., 2006, "Vertical Single- and Double-Walled Carbon Nanotubes Grown From Modified Porous Anodic Alumina Templates," Nanotechnology, **17**(15), pp. 3925–3929.
[7] Kang, S. J., Kocabas, C., Ozel, T., Shim, M., Pimparkar, N., Alam, M. A., Rotkin, S. V., and Rogers, J. A., 2007, "High-Performance Electronics Using Dense, Perfectly Aligned Arrays of Single-Walled Carbon Nanotubes," Nat. Nanotechnol., **2**(4), pp. 230–236.
[8] Nunes, C., Teixeira, V., Collares-Pereira, M., Monteiro, A., Roman, E., and Martin-Gago, J., 2002, "Deposition of Pvd Solar Absorber Coatings for High-Efficiency Thermal Collectors," Vacuum, **67**(3-4), pp. 623–627.
[9] Wang, Y., Kempa, K., Kimball, B., Carlson, J. B., Benham, G., Li, W. Z., Kempa, T., Rybczynski, J., Herczynski, A., and Ren, Z. F., 2004, "Receiving and Transmitting Light-Like Radio Waves: Antenna Effect in Arrays of Aligned Carbon Nanotubes," Appl. Phys. Lett., **85**(13), pp. 2607–2609.
[10] Itkis, M. E., Borondics, F., Yu, A. P., and Haddon, R. C., 2006, "Bolometric Infrared Photoresponse of Suspended Single-Walled Carbon Nanotube Films," Science, **312**(5772), pp. 413–416.
[11] Mizuno, K., Ishii, J., Kishida, H., Hayamizu, Y., Yasuda, S., Futaba, D. N., Yumura, M., and Hata, K., 2009, "A Black Body Absorber From Vertically Aligned Single-Walled Carbon Nanotubes," Proc. Natl. Acad. Sci. U.S.A., **106**(15), pp. 6044–6047.
[12] Maschmann, M. R., Franklin, A. D., Sands, T. D., and Fisher, T. S., 2007, "Optimization of Carbon Nanotube Synthesis From Porous Anodic Al-Fe-Al Templates," Carbon, **45**(11), pp. 2290–2296.
[13] Patil, N., Deng, J., Mitra, S., and Wong, H. S. P., 2009, "Circuit-Level Performance Benchmarking and Scalability Analysis of Carbon Nanotube Transistor Circuits," IEEE Trans. Nanotechnol., **8**(1), pp. 37–45.
[14] Li, Z. M., Tang, Z. K., Liu, H. J., Wang, N., Chan, C. T., Saito, R., Okada, S., Li, G. D., Chen, J. S., Nagasawa, N., and Tsuda, S., 2001, "Polarized Absorption Spectra of Single-Walled 4 Angstrom Carbon Nanotubes Aligned in Channels of an Alpo4-5 Single Crystal," Phys. Rev. Lett., **87**(12), p. 127401.
[15] Lidorikis, E., and Ferrari, A. C., 2009, "Photonics With Multiwall Carbon Nanotube Arrays," ACS Nano, **3**(5), pp. 1238–1248.
[16] Spataru, C. D., Ismail-Beigi, S., Benedict, L. X., and Louie, S. G., 2004, "Excitonic Effects and Optical Spectra of Single-Walled Carbon Nanotubes," Phys. Rev. Lett., **92**(7), p. 077402.
[17] Saito, R., Dresselhaus, G., and Dresselhaus, M. S., 1998, *Physical Properties of Carbon Nanotubes*, Imperial College Press, London.
[18] Ando, T., 1997, "Excitons in Carbon Nanotubes," J. Phys. Soc. Jpn., **66**(4), pp. 1066–1073.
[19] Rohlfing, M., and Louie, S. G., 2000, "Electron-Hole Excitations and Optical Spectra From First Principles," Phys. Rev. B, **62**(8), pp. 4927–4944.
[20] Hybertsen, M. S., and Louie, S. G., 1986, "Electron Correlation in Semiconductors and Insulators—Band-Gaps and Quasi-Particle Energies," Phys. Rev.ew B, **34**(8), pp. 5390–5413.
[21] Ch. Hafner, J. Smajic, M. Agio, 2010, "Numerical Methods for the Electrodynamic Analysis of Nanostructures," *Nanoclusters and Nanostructured Surfaces*, A. K. Ray, ed., Stevenson Ranch, CA: American Scientific Publishers, Valencia, CA.
[22] Stanton, J. F., Bartlett, R. J., 2003, "The Equation of Motion Coupled-Cluster Method. A Systematic Biorthogonal Approach to Molecular Excitation Energies, Transition Probabilities and Excited State Properties," J. Chem. Phys., **98**(9), pp. 7029–7039.
[23] Dreuw, A., Head-Gordon, M., 2005, "Single-Reference Ab Initio Methods for the Calculation of Excited States of Large Molecules," Chem. Rev., **105**(11), pp. 4009–4037.
[24] Burke, K., Weschnik, J., Gross, E. K. U., 2005, "Time-Dependent Density Functional Theory: Past, Present and Future," J. Chem. Phys., **123**(6), p. 062206
[25] Troullier, N., and Martins, J. L., 1991, "Efficient Pseudopotentials for Plane-Wave Calculations," Phys. Rev. B, **43**(3), pp. 1993–2006.
[26] Ismail-Beigi, S., 2006, "Truncation of Periodic Image Interactions for Confined Systems," Phys. Rev. B, **73**(23), p. 233103.
[27] Koledintseva, M. Y., Wu, J., Zhang, J. M., Drewniak, J. L., and Rozanov, K. N., 2004, "Representation of Permittivity for Multiphase Dielectric Mixtures in FDTD Modeling," 2004 International Symposium on Electromagnetic Compatibility, Symposium Record 1-3, pp. 309–314.
[28] Bachilo, S. M., Strano, M. S., Kittrell, C. Hauge, R. H., Smalley, R. R., Weisman, R. B., 2002, "Structure-Assigned Optical Spectra of Single-Walled Carbon Nanotubes," Science, **298**(5602) pp. 2361–2366
[29] Deslippe, J., Spataru, C. D., Prendergast, D., and Louie, S. G., 2007, "Bound Excitons in Metallic Single-Walled Carbon Nanotubes," Nano Lett., **7**(6), pp. 1626–1630.
[30] Fantini, C., Jorio, A., Souza, M., Strano, M. S., Dresselhaus, M. S., and Pimenta, M. A., 2004, "Optical Transition Energies for Carbon Nanotubes From Resonant Raman Spectroscopy: Environment and Temperature Effects," Phys. Rev. Lett., **93**(14), p. 147406.
[31] Ajiki, H., and Ando, T., 1994, "Aharonov-Bohm Effect in Carbon Nanotubes," Physica B, **201**, pp. 349–352.
[32] Kozinsky, B., and Marzari, N., 2006, "Static Dielectric Properties of Carbon Nanotubes From First Principles," Phys. Rev. Lett., **96**(16), p. 166801.
[33] Marinopoulos, A. G., Reining, L., Rubio, A., and Vast, N., 2003, "Optical and Loss Spectra of Carbon Nanotubes: Depolarization Effects and Intertube Interactions," Phys. Rev. Lett., **91**(4), p. 046402.
[34] Murakami, Y., Einarsson, E., Edamura, T., and Maruyama, S., 2005, "Polarization Dependence of the Optical Absorption of Single-Walled Carbon Nanotubes," Phys. Rev. Lett., **94**(8), p. 087402.
[35] Garcia-Vidal, F. J., Pitarke, J. M., and Pendry, J. B., 1997, "Effective Medium Theory of the Optical Properties of Aligned Carbon Nanotubes," Phys. Rev. Lett., **78**(22), pp. 4289–4292.
[36] Datta, S., Chan, C. T., Ho, K. M., and Soukoulis, C. M., 1993, "Effective Dielectric-Constant of Periodic Composite Structures," Phys. Rev. B, **48**(20), pp. 14936–14943.
[37] Einarsson, E., Murakami, Y., Kadowaki, M., Duong, H. M., Inoue, M., and Maruyama, S., 2006, "Production and Applications of Vertically Aligned Single-Walled Carbon Nanotubes," Therm. Sci. Eng., **14**(3), pp. 47–49.